The Astrophysical Journal, 809:140 (8pp), 2015 August 20 doi:10.1088/0004-637X/809/2/140

NuSTAR DISCOVERY OF AN UNUSUALLY STEADY LONG-TERM SPIN-UP OF THE Be BINARY 2RXP J130159.6–635806

Roman A. Krivonos[1,2], Sergey S. Tsygankov[2,3], Alexander A. Lutovinov[2], John A. Tomsick[1], Deepto Chakrabarty[4], Matteo Bachetti[5,6], Steven E. Boggs[1], Masha Chernyakova[7,8], Finn E. Christensen[9], William W. Craig[1,10], Felix Fürst[11], Charles J. Hailey[12], Fiona A. Harrison[11], George B. Lansbury[13], Farid Rahoui[14,15], Daniel Stern[16], and William W. Zhang[17]

[1] Space Science Lab, University of California, Berkeley, CA 94720, USA
[2] Space Research Institute, Russian Academy of Sciences, Profsoyuznaya 84/32, 117997 Moscow, Russia
[3] Tuorla Observatory, Department of Physics and Astronomy, University of Turku, Väisäläntie 20, FI-21500 Piikkiö, Finland
[4] MIT Kavli Institute for Astrophysics and Space Research, Cambridge, MA 02139, USA
[5] Observatoire Midi-Pyrénées, Université de Toulouse III—Paul Sabatier, F-31400 Toulouse, France
[6] CNRS, Institut de Recherche en Astrophysique et Planetologie, F-31028 Toulouse, France
[7] Dublin City University, Dublin 9, Ireland
[8] Dublin Institute for Advanced Studies, 31 Fitzwilliam Place, Dublin 2, Ireland
[9] DTU Space—National Space Institute, Technical University of Denmark, Elektrovej 327, DK-2800 Lyngby, Denmark
[10] Lawrence Livermore National Laboratory, Livermore, CA 94550, USA
[11] Cahill Center for Astronomy and Astrophysics, California Institute of Technology, Pasadena, CA 91125, USA
[12] Columbia Astrophysics Laboratory, Columbia University, New York, NY 10027, USA
[13] Department of Physics, University of Durham, South Road, Durham DH1 3LE, UK
[14] European Southern Observatory, K. Schwarzschild-Str. 2, D-85748 Garching bei München, Germany
[15] Department of Astronomy, Harvard University, 60 Garden Street, Cambridge, MA 02138, USA
[16] Jet Propulsion Laboratory, California Institute of Technology, Pasadena, CA 91109, USA
[17] NASA Goddard Space Flight Center, Greenbelt, MD 20771, USA
Received 2015 May 27; accepted 2015 July 16; published 2015 August 18

ABSTRACT

We present spectral and timing analyses of *Nuclear Spectroscopic Telescope Array* (*NuSTAR*) observations of the accreting X-ray pulsar 2RXP J130159.6–635806. The source was serendipitously observed during a campaign focused on the gamma-ray binary PSR B1259–63 and was later targeted for a dedicated observation. The spectrum has a typical shape for accreting X-ray pulsars, consisting of a simple power law with an exponential cutoff starting at ∼7 keV with a folding energy of $E_{\rm fold} \simeq 18$ keV. There is also an indication of the presence of a 6.4 keV iron line in the spectrum at the $\sim 3\sigma$ significance level. *NuSTAR* measurements of the pulsation period reveal that the pulsar has undergone a strong and steady spin-up for the last 20 years. The pulsed fraction is estimated to be ∼80%, and is constant with energy up to 40 keV. The power density spectrum shows a break toward higher frequencies relative to the current spin period. This, together with steady persistent luminosity, points to a long-term mass accretion rate high enough to bring the pulsar out of spin equilibrium.

Key words: pulsars: individual (2RXP J130159.6–635806) – stars: emission-line, Be – X-rays: binaries

1. INTRODUCTION

2RXP J130159.6–635806, first discovered by the *ROSAT* observatory, was later rediscovered in hard-X-rays by the *INTEGRAL*/IBIS telescope and designated with the name IGR J13020–6359 (Bird et al. 2006; Revnivtsev et al. 2006). The first comprehensive analysis of the temporal and spectral X-ray properties of this source was done by Chernyakova et al. (2005) using data from the *ASCA*, *BeppoSAX*, *INTEGRAL*, and *XMM-Newton* observatories. In particular, *XMM-Newton* data showed coherent pulsations with a period of around 700 s. Joint spectral analysis of *XMM-Newton* and *INTEGRAL* data demonstrated that the spectral shape is very typical for accretion-powered X-ray pulsars (namely, an absorbed power law with a high-energy cut-off).

Based on 2MASS archival data, Chernyakova et al. (2005) proposed that the binary companion of 2RXP J130159.6–635806 is a Be star at a distance of 4–7 kpc. Masetti et al. (2006) determined an optical counterpart with a prominent narrow Hα line at redshift zero superimposed on a very reddened continuum, suggesting a Galactic object, most likely a high mass X-ray binary hosting a late O-/early B-type star. This suggestion was later confirmed by Coleiro et al. (2013), who reported the presence of emission lines of He I λ2.0594 μm and Br (7–4) λ2.1663 μm, which are typical for a Be star. The spectral type of the optical counterpart was determined to be B0.5Ve. The orbital period of the binary remains unknown.

X-ray pulsars in binary systems with Be companions (BeXRPs) typically manifest themselves as transient sources through either Type I (periodic flares related to the periastron passage) or Type II outbursts (powerful rare transient events), or a combination of both (e.g., Reig 2011). 2RXP J130159.6–635806 shows several differences from a standard transient BeXRP. Specifically, it has a relatively low persistent flux, a long pulse period, and it does not demonstrate either Type I or Type II outbursts. Chernyakova et al. (2005), however, did report some variability of its X-ray flux.

Therefore, there are substantial reasons to consider 2RXP J130159.6–635806 as a member of the subclass of persistent BeXRPs (Reig & Roche 1999). So far, only a few members of this relatively small category of objects have been studied in detail: 4U 0352+309/X Persei, RX J0146.9+6121/LS I+61 235, RX J0440.9+4431, and RX J1037.5–564 (Haberl et al. 1998; Reig & Roche 1999).

Table 1
NuSTAR Observations

Seq. Num.	Obs. ID	Start Time (UTC)	Exp. (ks)	Net Count Rate[a] (counts s^{-1})		Period[b] (s)
1	30002017004	2014 May 04 10:01	33.3	$(1.49 \pm 0.02) \times 10^{-1}$	$(2.94 \pm 0.03) \times 10^{-1}$	643.68 ± 0.02
2	30002017008	2014 Jun 02 19:21	26.4	$(2.00 \pm 0.12) \times 10^{-2}$	$(7.41 \pm 0.20) \times 10^{-2}$	643.64 ± 0.30
3	30002017010	2014 Jun 14 17:21	29.1	$(7.05 \pm 0.19) \times 10^{-2}$	$(1.62 \pm 0.03) \times 10^{-1}$	643.14 ± 0.18
4	30001032002	2014 Jun 24 00:06	31.6	1.342 ± 0.007	1.239 ± 0.007	642.90 ± 0.01

Notes. The target for the first three observations was PSR B1259–63, which placed 2RXP J130159.6–635806 offset by 9.′55 from the optical axis. The fourth observation was taken with 2RXP J130159.6–635806 on-axis.
[a] Net count rate in 3–78 keV band for FPMA and FPMB extracted from a circular region with a radius of 120″.
[b] Measured pulsation period for 2RXP J130159.6–635806.

In this paper, we present results of a comprehensive analysis of the temporal and spectral properties of 2RXP J130159.6–635806 in a broad energy range, finding some properties that are very unusual for BeXRPs. All errors are quoted at the 90% confidence level unless otherwise stated.

2. OBSERVATIONS

2RXP J130159.6–635806 was initially serendipitously observed with the *Nuclear Spectroscopic Telescope Array* (*NuSTAR*; Harrison et al. 2013) during observations of the gamma-ray binary PSR B1259–63, with three data sets taken in 2014 May–June (King et al. 2015). In one observation, 2RXP J130159.6–635806 appears in the corner of $\sim 13' \times 13'$ *NuSTAR*'s field of view (FOV), and, in two more, the source is at the extreme edge of the FOV. Despite the large off-axis angles, the *NuSTAR* data were successfully used to extract coherent pulsations. This motivated the *NuSTAR* team to trigger an on-axis 30 ks observation of 2RXP J130159.6–635806 in order to obtain high-quality data for spectral and timing analysis. Table 1 lists the *NuSTAR* observations used in this work.

NuSTAR carries two co-aligned identical X-ray telescopes operating in the wide energy band from 3 to 79 keV with an angular resolution of 18″ (FWHM) and half-power diameter of 58″. Spectral resolution of 400 eV (FWHM) at 10 keV is provided by independent focal planes for each telescope, usually referred to as focal plane modules A and B (FPMA and FPMB).

NuSTAR data can have systematic positional offsets as high as 10″. Prior to extraction, we therefore corrected the world coordinate system of the event files for the four observations to match the PSR B1259–63 and 2RXP J130159.6–635806 centroid positions based on cataloged coordinates.

Since the *NuSTAR* point-spread function (PSF) has wide wings (Harrison et al. 2013; An et al. 2014), we investigated how the surface brightness of the source changes with radius in order to determine regions where the source dominates over the background. We found that 2RXP J130159.6–635806 is well above background within 120″ ($\sim$92% of PSF enclosed energy; see, e.g., An et al. 2014), and that the background count rate can be robustly measured at radii $\geqslant$ 200″ from the source. Taking this into consideration, we defined the corresponding extraction regions shown in Figure 1 for the fourth (on-axis) observation. The other three observations, for which 2RXP J130159.6–635806 is far off-axis, have been treated similarly. Following *NuSTAR* recommended standard practice, we chose the background regions to be on the same detector chip as the source.

3. TIMING ANALYSIS

2RXP J130159.6–635806 is a known source of coherent X-ray pulsations at a period of $\sim$700 s with an average spin-up rate of $\dot{\nu} \simeq 2 \times 10^{-13}$ Hz s^{-1} (Chernyakova et al. 2005). We performed timing analysis of the *NuSTAR* data using the XRONOS (epoch folding tool efsearch; Leahy et al. 1983) after barycentering the data with *barycorr*. For each *NuSTAR* observation, the pulse period and its uncertainty were calculated following the procedure described in (Boldin et al. 2013). Namely, a large number (10^4) of source light curves were simulated, the pulse period of each one was determined with efsearch, and the distribution of the corresponding pulse periods was constructed. The mean value of this distribution and its standard deviation were taken as the pulse period and its 1σ uncertainty, correspondingly. Table 1 lists period results derived from the FPMA and FPMB combined light curves. The inset of Figure 2 shows the evolution of the spin period as a function of time.

As seen from Table 1 and Figure 2, all four *NuSTAR* data sets are suitable for pulsation detection. It is also quite evident that periods recorded over the time span of 50 days are not consistent with each other, clearly showing a decrease in the period. We utilized the first and fourth *NuSTAR* observations, which have the most accurate period measurements and also span the full duration of the *NuSTAR* coverage, to measure a period derivative of $\dot{P} = -0.0154(5)$ s day^{-1}, equivalent to $-1.78(6) \times 10^{-7}$ s s^{-1}, or $\dot{\nu} \simeq 4.3 \times 10^{-13}$ Hz s^{-1}. This is in agreement with the Chernyakova et al. (2005) spin-up measurement of the second interval of their data, after the "break" at MJD $\sim$51900 ($\dot{\nu} \simeq 4 \times 10^{-13}$ Hz s^{-1}). This is quite remarkable since there is almost a decade between the period measurements.

3.1. Pulse Period Long-term Evolution

2RXP J130159.6–635806 regularly fell into the FOV of various X-ray telescopes thanks to extensive observational campaigns dedicated to PSR B1259–63 which is located only 9.′55 away. This allows us to investigate the long-term evolution of the pulse period. We analyzed the *XMM-Newton* (Jansen et al. 2001) archival data from 2007–2011 using the procedures described by Chernyakova et al. (2005) and Science Analysis Software version 14.0.0. The list of selected *XMM-Newton* observations with corresponding period measurements are shown in Table 2.

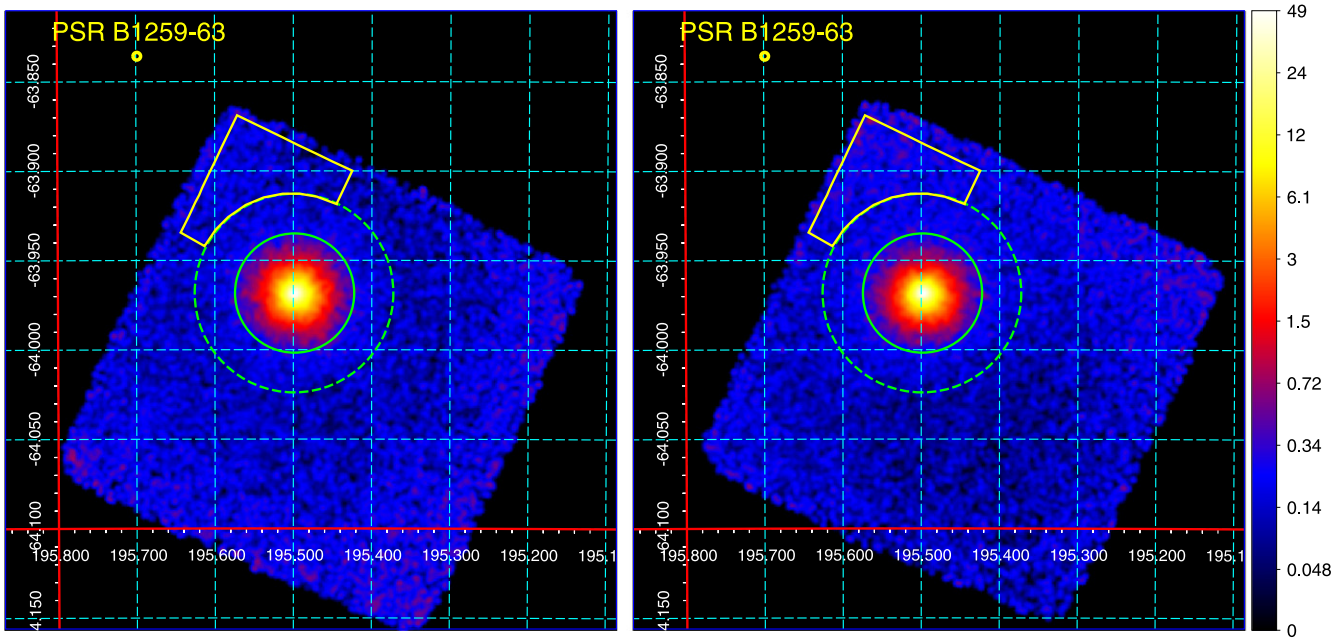

Figure 1. Exposure-corrected FPMA (left) and FPMB (right) images of 2RXP J130159.6–635806 for the fourth observation in the 3–78 kev band. The images have been smoothed by a Gaussian kernel with 3 pixel width (1 pixel = 3″). Each image is color-coded in logarithmic scale. The color bar on the right shows the units of the images expressed in 10^{-4} cts pixel^{-1} s^{-1}. The solid green circle (120″ radius) and the yellow shape denote regions for the source and background extraction, respectively. The dashed green circle demonstrates an angular distance of 200″ from the target. The position of the nearby bright source PSR B1259–63 is indicated.

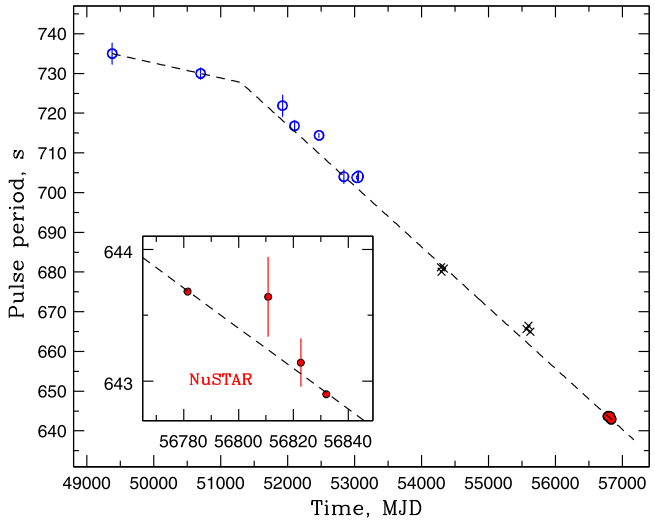

Figure 2. Evolution of the pulse period as a function of time. Blue circles show period measurements published by Chernyakova et al. (2005) using *ASCA*, *BeppoSAX*, and *XMM-Newton* data; values obtained in this work are shown by black crosses and red points for data from *XMM-Newton* and *NuSTAR*, respectively. Dashed lines represent linear fits to the period evolution with two different spin-up rates (see the text for details).

Table 2
XMM-Newton Observations

Obs. ID	Start Time (UTC)	Exp. (ks)	Period (s)
0504550501	2007 Jul 08 12:01	14.1	681.20 ± 0.15
0504550601	2007 Jul 16 19:59	55.3	680.06 ± 0.10
0504550701	2007 Aug 17 08:38	11.4	680.87 ± 0.20
0653640401	2011 Jan 06 17:37	19.9	665.65 ± 0.20
0653640501	2011 Feb 02 18:59	26.3	666.50 ± 0.20
0653640601	2011 Mar 04 05:59	12.9	664.95 ± 0.20

Figure 2 presents the long-term evolution of the period, showing that the 2RXP J130159.6–635806 neutron star has undergone very strong and steady spin-up during the last 20 years. The first available value of spin period, measured in 1994, is 735 s (Chernyakova et al. 2005). The most recent measurements by *NuSTAR*, from 2014, show the period to be around 643 s (Table 1). This means that during the last ∼20 years the spin period decreased by ∼92 s, corresponding to a mean spin-up rate of $\sim 1.4 \times 10^{-7}$ s s^{-1}. Figure 2 shows a change in the average spin-up rate, first reported by Chernyakova et al. (2005).

We approximated the long-term period evolution with a linear function with one change in slope. A fit shows that the break occurred at MJD 51300 ± 217 (mid 1999) with a spin-up rate before and after the break of $(4.3 \pm 2.7) \times 10^{-8}$ s s^{-1} and $(1.774 \pm 0.003) \times 10^{-7}$ s s^{-1}, respectively. As seen from the fit parameters, the spin-up rate becomes significantly higher after the break. As noted above, the inset of Figure 2 shows that the *NuSTAR* data points fit the long-term spin-up rate with remarkably high precision.

Similar behavior was observed for the X-ray pulsar GX 1 + 4, which showed steady spin up for more than a decade (see, e.g., Bildsten et al. 1997; González-Galán et al. 2012). However, GX 1 + 4 belongs to the subclass of accreting X-ray pulsars known as symbiotic X-ray binaries. For BeXRPs, persistent sources typically demonstrate pulse periods that are relatively stable. Examples include the population of Be systems in the Small Magellanic Cloud (Klus et al. 2014) and the well-known low luminosity Galactic system X Persei (Lutovinov et al. 2012). Transient BeXRPs show strong spin-up during Type I and Type II outbursts (Bildsten et al. 1997) with significant spin-down episodes in between (see, e.g., Postnov et al. 2015). Therefore, 2RXP J130159.6–635806 is a unique source among the BeXRPs because it demonstrates steady and high long-term spin-up with a relatively low and stable luminosity.

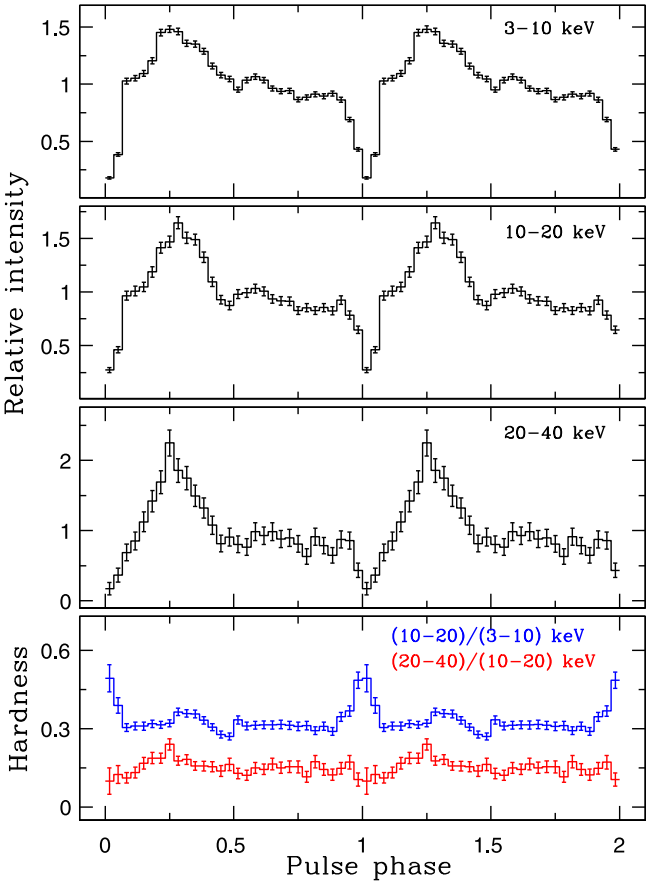

Figure 3. *NuSTAR*2RXP J130159.6–635806 pulse profiles in three energy bands (3–10, 10–20, and 20–40 keV), normalized by the mean flux. The lower panel shows two hardness ratios, (10–20 keV)/(3–10 keV) and (20–40 keV)/(10–20 keV) in blue and red, respectively. The profiles are shown twice for clarity.

3.2. Pulse Profile and Pulsed Fraction

Pulsar pulse profiles and their evolution with luminosity and energy band depend on the geometrical and physical properties of the emitting regions in the vicinity of the neutron star. In Figure 3, the *NuSTAR* pulse profiles of 2RXP J130159.6–635806 are shown in three different energy bands: 3–10, 10–20, and 20–40 keV. The lower panel shows "soft" ((10–20)/(3–10) keV) and "hard" ((20–40)/(10–20) keV) hardness ratios.

At all energies, the pulse profile can roughly be divided into one main peak at phases 0.0–0.5 and two smaller peaks at phases 0.5–0.75 and 0.75–1.0. The main feature that changes with energy is the depth of the minimum at phase 0.0. As shown in the lower panel of Figure 3, while the "hard" hardness ratio is almost constant, the "soft" hardness ratio shows a maximum at phase 0.0 due to an increase in the depth of the minimum at 3–10 keV. Such behavior is caused by differences in the source spectrum with pulse phase (see Section 4).

Figure 4 shows the pulsed fraction as a function of energy. The pulsed fraction is defined as $\mathrm{PF} = (I_{\max} - I_{\min})/(I_{\max} + I_{\min})$, where $I_{\max}$ and $I_{\min}$ are the maximum and minimum intensities in the pulse profile, respectively. Defined in this way, the pulsed fraction is very high (about 80%). The alternative way to characterize the pulsed fraction is the relative root mean square

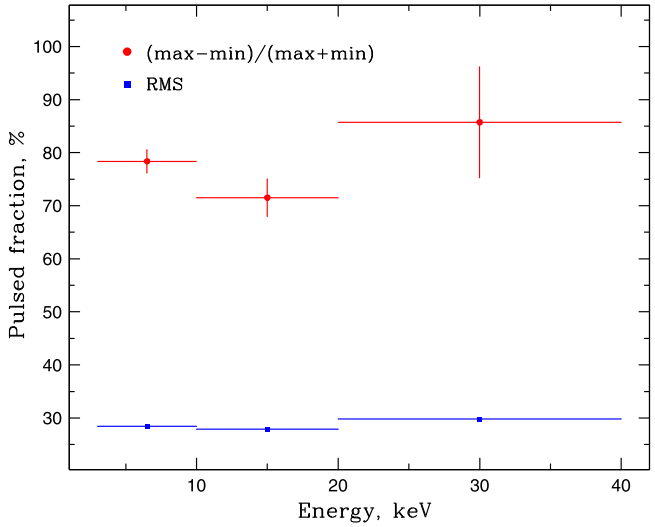

Figure 4. Pulsed fraction (red circles) and relative rms (blue squares) of 2RXP J130159.6–635806 obtained with *NuSTAR* as a function of energy.

(rms), which can be calculated using the following equation:

$$\mathrm{rms} = \frac{\left(\frac{1}{N}\sum_{i=1}^{N}\left(P_i - \langle P\rangle\right)^2\right)^{\frac{1}{2}}}{\langle P\rangle}, \quad (1)$$

where P_i is the background-corrected count rate in a given bin of the pulse profile, $\langle P\rangle$ is the count rate averaged over the pulse period, and N is the total number of phase bins in the profile ($N = 30$ in our analysis). The rms deviation obtained in this way reflects the variability of the source pulse profile in a manner that is not sensitive to outliers like the narrow features seen in the profile of 2RXP J130159.6–635806. Therefore, this quantity has a value of around 30%, which is much lower than the classically determined pulsed fraction and also independent of the energy band (see Figure 4).

It is interesting to note that in contrast to the majority of X-ray pulsars (Lutovinov & Tsygankov 2009), 2RXP J130159.6–635806 does not show an increase in the pulsed fraction at higher energies. Such uncharacteristic behavior was previously observed for another persistent BeXRP—RX J0440.9+4431 (Tsygankov et al. 2012). On the other hand, Figure 3 shows that the pulsed fraction increases somewhat with energy if $I_{\min}$ is defined from the the pulse plateau rather than from the pulse minimum. In other words, the peak-to-plateau difference slightly grows with energy.

3.3. Power Spectrum

The observed 20-year strong and steady spin-up of 2RXP J130159.6–635806 reveals the existence of a long-term accelerating torque, which indicates that the binary interaction must lead to regular accretion over a decade-long timescale, although this could certainly be episodic (e.g., at periastron passages). The torque can be transferred by matter accreted from either the disk around the neutron star or a stellar wind from the optical counterpart. Unfortunately, there is no strong observational evidence allowing us to distinguish between these two different accretion channels. In both scenarios, this process is defined mainly by the mass accretion rate and the magnetic field strength (see, e.g., Ghosh & Lamb 1979).

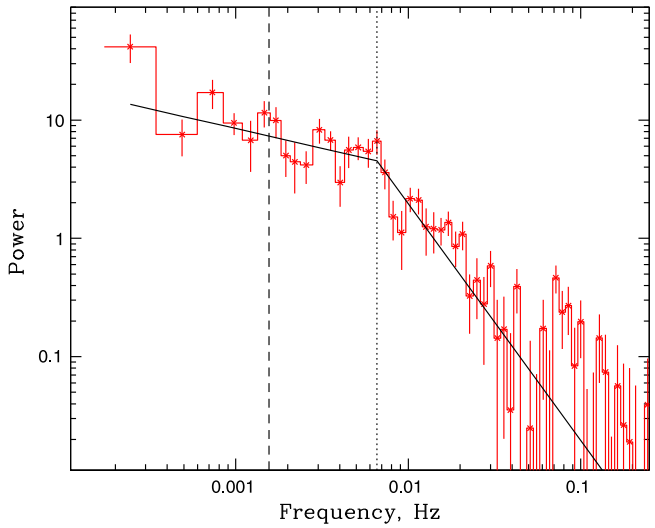

Figure 5. Noise power spectrum of 2RXP J130159.6–635806 obtained with the *NuSTAR* data in observation 30001032002 (red histogram; the fourth observation). The solid line shows a broken power-law model with the fitted value of the break frequency, 0.0066 Hz (vertical dotted line). The power-law slope above the break is fixed to −2. The position of the pulse frequency (0.0015 Hz) is shown by the vertical dashed line.

Due to the unknown distance of 2RXP J130159.6–635806, the luminosity and mass accretion rate are highly uncertain; the magnetic field is also unknown since no cyclotron line is found in the energy spectrum (Section 4). However, some qualitative conclusions about the interaction between the accretion disk and the neutron star magnetosphere can be made from the noise power spectrum of the X-ray pulsar.

According to the "perturbation propagation" model, stochastic variations of viscous stresses in the accretion disk cause variations of the mass accretion rate (Lyubarskii 1997; Churazov et al. 2001). This, in turn, results in a specific shape of the Power Density Spectrum (PDS) of the emerging light curve. Namely, it will appear as a power law with slope –1 to −1.5 (but the exact value is not well established for X-ray pulsars) up to the break frequency, which is the highest frequency that can be generated in the accretion disk (Lyubarskii 1997).

In the case of a highly magnetized neutron star, this maximal frequency is limited by the Keplerian frequency at the magnetospheric radius, above which one can expect a cutoff in the source PDS (Revnivtsev et al. 2009). If the source stays in spin equilibrium (corotation), the cutoff frequency will coincide with the spin frequency of the pulsar, whereas, in the case of spin-up (increased mass accretion rate), the magnetosphere will be squeezed and additional noise will be generated at higher frequencies. If the mass accretion rate is known (i.e., the distance to the source is known), this property of the PDS can be used to estimate the magnetic field strength of the neutron star (Revnivtsev et al. 2009; Tsygankov et al. 2012; Doroshenko et al. 2014). The appearance of the break in the PDS does not necessarily indicate that accretion is from a disk. There are wind-accreting sources in spin equilibrium also showing a break in their PDSs around the pulse frequency (Hoshino & Takeshima 1993). However, the evolution of the PDS shape as a function of mass accretion rate in such systems is not well studied.

In Figure 5, we show the PDS of 2RXP J130159.6–635806 obtained with the *NuSTAR* data in the fourth observation after subtracting the pulse profile folded with the measured period from the light curve. The solid line represents the fitting model in the form of a broken power law. The measured break frequency is 0.0066 Hz (shown by dotted line), and it is clear that it is shifted toward higher frequencies relative to the spin frequency in this observation (0.0015 Hz; shown by dashed vertical line). The power-law slope above the break frequency is fixed at –2 (Revnivtsev et al. 2009). The best-fit value of the slope below the break is −0.33. Given the steady persistent luminosity, we conclude that the spin-up observed during the last ∼20 years is caused by a long-term mass accretion rate that is high enough to squeeze the magnetosphere inside the corotational radius. This finding confirms the uniquness of 2RXP J130159.6–635806 among the other X-ray pulsars in binary systems with Be companions.

4. SPECTRAL ANALYSIS

We used *nuproducts*, a part of the NuSTARDAS package, to extract source and background spectra and to generate *NuSTAR* response matrix (RMF) and effective area (ARF) files for a point source. In our analysis, we utilized the most recent calibration database (CALDB), version 20150316. The extracted spectra were then grouped to have more than 20 counts per bin using the *grppha* tool from the HEAsoft 6.15.1 package. We fit the *NuSTAR* spectra using XSPEC version 12.8.1 (Arnaud 1996).

4.1. Pulse Phase-averaged Spectroscopy

According to measurements from the *ASCA* and *XMM-Newton* observatories, the spectrum of 2RXP J130159.6–635806 is characterized by a moderate absorption value $N_{\rm H} = (2.48 \pm 0.07) \times 10^{22}\,{\rm cm}^{-2}$, which is stable over a dozen years (Chernyakova et al. 2005). This value was obtained by approximating the source spectra as a power-law model modified by interstellar absorption (wabs model in the XSPEC package). Note that it is just slightly higher than the value of the interstellar hydrogen absorption $(1.7–1.9) \times 10^{22}\,{\rm cm}^{-2}$ determined by Dickey & Lockman (1990) in the direction of 2RXP J130159.6–635806.

In the first three *NuSTAR* observations, 2RXP J130159.6–635806 serendipitously appeared highly offset from the optical axis, and at the large off-axis angles the absolute flux measurements can be affected by inaccurate PSF positioning and subsequent inapropriate weighting in the spectrum extraction procedure. This leads to large systematics for the extracted spectra. Therefore, we restrict detailed analysis of the source spectrum to the data obtained in the fourth (on-axis) observation, which provides high-quality data.

In general, the spectrum of 2RXP J130159.6–635806 has a shape that is typical for accreting pulsars in binary systems, showing a hard spectrum with an exponential cutoff at high energies. Figure 6(a) presents the phase-averaged spectrum approximated with the most suitable spectral model determined below. We initially modeled data with a cutoff power-law model (CUTOFFPL in the XSPEC package)

$$AE^{-\Gamma}e^{-\frac{E}{E_{\rm fold}}}, \quad (2)$$

where Γ is the photon index, $E_{\rm fold}$ is the characteristic energy of the cutoff (e.g., the folding energy), and A is a normalization. This model was modified by interstellar absorption in the form of the WABS model. As the working energy range of the

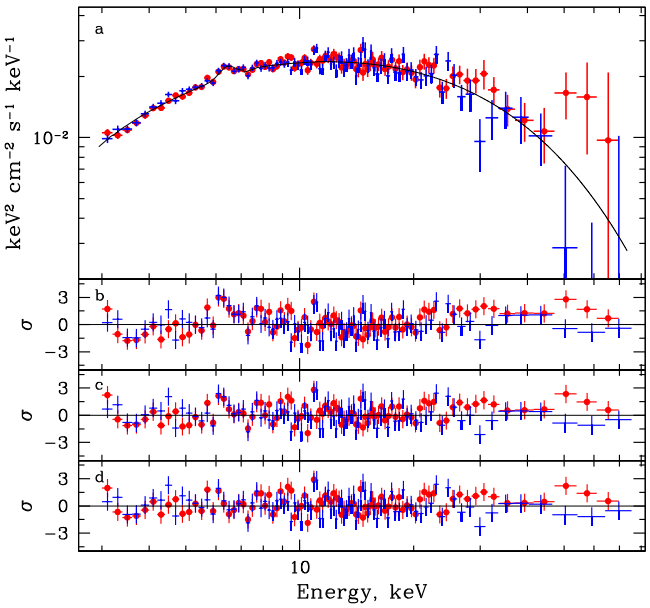

Figure 6. Top panel (a): pulse phase-averaged spectrum of 2RXP J130159.6–635806 obtained with *NuSTAR* during the fourth observation. Red points and blue crosses show module A and B data, respectively. The black line represents the best fit by the "highecut" model with an iron emission line at 6.4 keV. Bottom panels (b)–(d) show corresponding residuals from the models "cutoff," "highecut," and "highecut" with the 6.4 keV line, respectively (see the text and Table 3).

NuSTAR observatory begins at 3 keV, it is not very sensitive to measuring low absorption columns. Therefore, in the following analysis, the interstellar absorption was fixed to the value $N_{\rm H} = 2.48 \times 10^{22}\,{\rm cm}^{-2}$ measured by Chernyakova et al. (2005). Note that we simultaneously fitted spectra obtained by both *NuSTAR* modules. To take into account the uncertainty in their relative calibrations, which may be even more of a concern for the observations where the source is highly offset from the optical axis, we added a cross-calibration constant between the modules. The fitting parameters for different data sets are shown in Table 3.

The "cutoff" model approximates the source spectrum relatively well with $\chi^2 = 992.18$ for 921 degrees of freedom (dof; see Table 3). Nevertheless, a wave-like structure is clearly seen in the residual panel Figure 6(b). To improve the quality of the fit, we applied another continuum model in the form of a power-law multiplied by a high-energy cutoff (HIGHECUT model in the XSPEC package; White et al. 1983). This model can be written as

$$AE^{-\Gamma} \times \begin{cases} 1 & \left(E \leqslant E_{\rm cut}\right) \\ e^{-(E-E_{\rm cut})/E_{\rm fold}} & \left(E > E_{\rm cut}\right), \end{cases} \quad (3)$$

where $E_{\rm cut}$ is the energy where the cutoff starts. As in the previous case, we fixed the interstellar absorption value. Residuals of modeling the source spectrum with "highecut" are presented in Figure 6(c), and best-fit parameters are listed in Table 3. The "highecut" model significantly improves the quality of the fit ($\chi^2 = 929.72$ for 920 dof). The high-energy cutoff value $E_{\rm cut}$ is found to be $6.48^{+0.22}_{-0.15}$ keV, which is significantly lower than the value of ∼25 keV reported by Chernyakova et al. (2005) using simultaneous *XMM-Newton* and *INTEGRAL* data. The apparent discrepancy is probably due to the lower statistical quality of the *INTEGRAL* data and the gap between the energy bands covered by the *XMM-Newton* and *INTEGRAL* observatories. An additional possible problem is that the cutoff energy $E_{\rm cut} = 6.48$ keV is very close to the energy of the iron fluorescent line at 6.4 keV. The simplistic "highecut" model might hide the presence of the emission line in the source spectrum. Observed deviations of the measured spectrum from the model near this energy argue in favor of this possibility.

To investigate this issue, we added a Gaussian emission line to the "highecut" model, fixing its energy to 6.4 keV and width to 0.1 keV, allowing its normalization to be a free parameter. This resulted in an additional improvement of the fit to $\chi^2 = 916.97$ for 919 dof for a normalization of $(2.31 \pm 0.70) \times 10^{-5}\,{\rm ph\,cm^{-2}\,s^{-1}}$. The corresponding equivalent width of the line is ${\rm EW} = 44^{+48}_{-32}$ eV (3σ error). We determined the significance of the line using the XSPEC script *simftest* with 4×10^4 trials, and found that presumption against the null hypothesis, or no line required by the data is 3×10^{-3}, which corresponds to $\sim 3\sigma$ line detection, assuming a normal distribution. The residuals of the "highecut" model with the 6.4 keV iron line are shown in Figure 6(d). The model itself, together with spectral data points, is shown in Figure 6(a).

Considering the moderate spectral resolution of the *NuSTAR* observatory and the low significance of the detected iron line, we investigated the possibility of the presence of an iron fluorescence line in the *XMM-Newton* spectrum of 2RXP J130159.6–635806. As mentioned above, the X-ray pulsar 2RXP J130159.6–635806 was observed with *XMM-Newton* many times during programs studying PSR B1259–63. For our purposes, we chose the two observations with the longest exposures—ObsID 0092820301 (∼41.2 ksec) and ObsID 0504550601 (∼55.3 ksec). As for the *NuSTAR* observations, we modeled the spectra of 2RXP J130159.6–635806, including the Gaussian line at 6.4 keV. For both of the *XMM-Newton* observations, we did not find a significant improvement in the fits when the iron line was added and obtained a conservative upper limit (3σ) for the equivalent width of the iron line of 110 eV, which is consistent with the *NuSTAR* results.

Despite the fact that the first three *NuSTAR* observations were made at large offset angles, and the corresponding statistics are significantly lower than for the fourth observation, some useful spectral information can still be extracted. For these observations, we used the same "highecut" model. Due to low statistics and poor fit, we fixed power-law slopes in the second and third data sets at a $\Gamma = 1.37$ value measured in the fourth observation. As seen from Table 3, where the best-fit parameters are listed, the principal parameters—power-law slope (Γ), cut-off energy ($E_{\rm cut}$), and folding energy ($E_{\rm fold}$)—of the first three high-offset observations are in general agreement with the fourth (on-axis) observation modeled with "highecut."

The estimated 2–10 keV flux of 2RXP J130159.6–635806 is about $3 \times 10^{-11}\,{\rm erg\,s^{-1}\,cm^{-2}}$ during our observations, which is in agreement with the value of $(2–3) \times 10^{-11}\,{\rm erg\,s^{-1}\,cm^{-2}}$ measured by Chernyakova et al. (2005). An absence of strong transient activity from 2RXP J130159.6–635806 on long timescales is confirmed with the *RXTE*/ASM and *Swift*/BAT instruments. Note that Chernyakova et al. (2005) reported on a flaring episode, but the flux of the flare was relatively low, rising by a factor of a few (up to $\sim 10^{-10}\,{\rm erg\,s^{-1}\,cm^{-2}}$).

Table 3
Parameters for the 2RXP J130159.6–635806 Phase-averaged Spectral Analysis Based on *NuSTAR* Observations

Seq. Num.	Model[a]	Const[b]	Photon Index	E_{cut} (keV)	E_{fold} (keV)	Flux[c] $_{2-10\ keV}$ FPMA	FPMB	χ^2_ν (dof)
1	HI	1.24 ± 0.02	$1.40^{+0.07}_{-0.14}$	$7.47^{+0.86}_{-1.55}$	$17.43^{+1.79}_{-1.29}$	$2.16^{+0.12}_{-0.38}$	$2.68^{+0.13}_{-0.48}$	1.06 (458)
2	HI	0.61 ± 0.04	1.37 (frozen)	$5.72^{+0.65}_{-1.90}$	$15.49^{+2.62}_{-1.73}$	$3.29^{+0.26}_{-1.47}$	$2.01^{+0.04}_{-0.95}$	0.92 (124)
3	HI	0.92 ± 0.03	1.37 (frozen)	$5.68^{+0.53}_{-0.62}$	$17.48^{+1.45}_{-1.35}$	$2.11^{+0.08}_{-0.13}$	$1.95^{+0.06}_{-0.10}$	0.81 (264)
4	CU	1.00 ± 0.01	1.04 ± 0.03	⋯	12.62 ± 0.48	$3.79^{+0.05}_{-0.10}$	$3.79^{+0.05}_{-0.11}$	1.07 (921)
	HI	1.00 ± 0.01	1.32 ± 0.03	$6.48^{+0.22}_{-0.15}$	$16.78^{+0.68}_{-0.56}$	$3.79^{+0.05}_{-0.10}$	$3.79^{+0.05}_{-0.11}$	1.01 (920)
	HI+Fe[d]	1.00 ± 0.01	1.37 ± 0.04	$6.94^{+0.50}_{-0.42}$	17.96 ± 0.87	$3.79^{+0.05}_{-0.10}$	$3.79^{+0.05}_{-0.11}$	1.00 (919)

Notes.
[a] The XSPEC spectral model used. "CU": WABS*CUTOFFPL, "HI": WABS*POWERLAW*HIGHECUT, "HI+Fe": WABS(POWERLAW*HIGHECUT+GAU).
[b] Constant factor of the FPMB spectrum relative to FPMA.
[c] The absorbed flux in units of 10^{-11} erg s^{-1} cm^{-2}.
[d] The corresponding 6.4 keV iron line parameters are: $\sigma = 0.1$ keV (fixed), normalization $(2.31 \pm 0.70) \times 10^{-5}$ ph cm^{-2} s^{-1}, and line equivalent width EW $= 44^{+48}_{-32}$ eV (3σ error).

Finally, in order to check for the possible presence of a cyclotron absorption line in the source spectrum, we modified the best-fit model (WABS*(POWERLAW*HIGHECUT+GAU)) by including an absorption feature in the form of a Lorentzian optical depth profile (CYCLABS model in XSPEC; Mihara et al. 1990). The search procedure was performed following the prescription from Tsygankov & Lutovinov (2005). Namely, we varied the energy of the line over the range between 5 and 50 keV with 3 keV steps and the line width between 2 and 12 keV with 2 keV steps, leaving the line depth as a free parameter. We did not find strong evidence for a cyclotron line in the spectrum of 2RXP J130159.6–635806 (no trials gave a significance higher than $\sim 2\sigma$).

4.2. Pulse Phase-resolved Spectroscopy

In order to study the evolution of the source spectrum over the pulse period, we performed pulse phase-resolved spectroscopy using the data from the fourth observation. The period was divided into 10 phase bins with the zero phase coinciding with the main minimum in the pulse profile. According to the pulse phase-averaged spectral analysis, the fitting model was chosen in the form of (WABS*(POWERLAW*HIGHECUT+GAU)). However, due to much lower statistics, the photon index was fixed at the value from the averaged spectrum ($\Gamma = 1.37$). We selected this parameter due to its virtual constancy over the pulse in our preliminary analysis of the same data. The N_H value is not very well constrained by the *NuSTAR* data; however we checked that it is consistent with being constant in phase, and we fixed it as well.

The results are shown in Figure 7. The average pulse profile of 2RXP J130159.6–635806 across the entire *NuSTAR* energy range is presented in the upper panel. The lower panels demonstrate the behavior of the two free spectral parameters: the cut-off energy (E_{cut}) and the folding energy (E_{fold}). The cut-off energy is quite stable over the pulse except at the pulse minimum where its value increases approximately by a factor of two. The folding energy demonstrates an apparent correlation with the pulse intensity, which is probably caused by increasing a spectral hardness around the pulse maximum. Such behavior of the spectral parameters over the pulse can explain the corresponding behavior of the hardness ratios constructed from the pulse profiles in different energy bands, previously shown in Figure 3. The (20–40)/(10–20) keV hardness ratio demonstrates correlation with the pulse intensity and the (10–20)/(3–10) keV ratio peaks at the pulse minimum right in place where E_{cut} shifts from ~7 to ~16 keV. Finally, it is necessary to note that the observed behavior of spectral parameters with the pulse phase can be caused by both physical and artificial reasons (in particular, due to limitations of available data, the adopted spectral model, and which model parameters were fixed). More data are required to confidently constrain all of the spectral parameters and trace their behavior with the pulse phase.

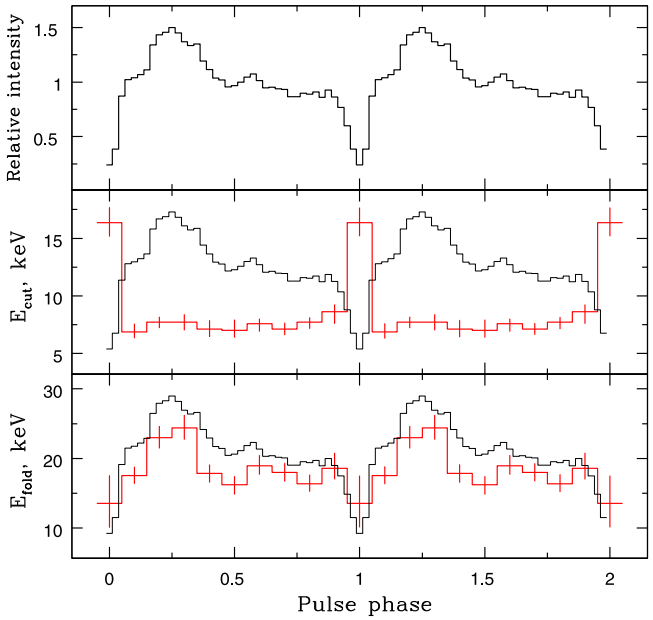

Figure 7. Parameters of the best-fit model (WABS*(POWERLAW*HIGHECUT+GAU)) as a function of pulse phase in the fourth (on-axis) observation. Top: the black histogram shows the pulse profile in the entire energy range (duplicated in the other two panels). Middle and bottom, respectively: cutoff energy (E_{cut}) and folding energy (E_{fold}).

5. SUMMARY

We summarize the results of spectral and timing analyses of serendipitous and dedicated *NuSTAR* observations of the

accreting X-ray pulsar 2RXP J130159.6–635806 in 2014 May–June.

1. The source demonstrates strong pulsations with a period of ∼640 s. The ∼80% pulsed fraction is measured to be constant with energy up to 40 keV.
2. The pulse profile is virtually independent of energy and can roughly be divided into one main peak at phases 0.0–0.5 and two smaller peaks at phases 0.5–0.75 and 0.75–1.0. The only feature that is changing with energy is the depth of the main minimum at phase 0.
3. The measured period shows a significant change over the ∼50 day time span of the *NuSTAR* observations, which is consistent with a spin-up rate of $\dot{\nu} \simeq 4.3 \times 10^{-13}$ Hz s^{-1}. This rate is in remarkable agreement with measurements made by Chernyakova et al. (2005) almost a decade ago.
4. Together with the results of Chernyakova et al. (2005), the *XMM-Newton* data taken in 2007 and 2011, and the *NuSTAR* observations, we show a long-term spin-up trend of the source during the last 20 years. During the last 15 years, the source has undergone a strong and steady spin-up rate at the level of $\dot{P} = (1.774 \pm 0.003) \times 10^{-7}$ s s^{-1}.
5. The PDS of the source shows a clear break at 0.0066 Hz, which is higher than the period frequency of 0.0015 Hz. This fact, together with the steady persistent luminosity of the source, implies that the spin-up observed during the last 20 years is likely caused by a long-term mass accretion rate high enough to squeeze the magnetosphere inside the corotational radius, which makes 2RXP J130159.6–635806 unique among other X-ray pulsars in binary systems with Be companions.
6. The phase-averaged spectrum of the source has a typical shape for accreting neutron stars in binary systems, in particular, for X-ray pulsars, and demonstrates an exponential cutoff at high energies. Our best-fit model contains an absorbed power-law with $\Gamma \simeq 1.4$, modified by a high-energy spectral drop with a cut-off energy of $E_{\rm cut} \simeq 7$ keV and a folding energy of $E_{\rm fold} \simeq 18$ keV. The spectrum also shows $\sim 3\sigma$ evidence for an iron 6.4 keV emission line, with an improvement in the fit when it is included.
7. The observed flux corresponds to an *unabsorbed* luminosity in the range $\sim(8\text{–}26) \times 10^{34}$ erg s^{-1}, assuming a source distance between 4 and 7 kpc (Chernyakova et al. 2005). These luminosity values imply that the source is a member of the subclass of persistent low luminosity Be systems (Reig 2011).
8. The phase-resolved spectroscopy shows some differences in source spectrum with phase. The cut-off energy is very stable over the pulse except at zero phase where its value increases by a factor of two. The apparent correlation of the folding energy with pulse intensity is attributed to the change in hardness of the source spectrum with orbital phase.

This research has made use of data obtained with *NuSTAR*, a project led by Caltech, funded by NASA and managed by NASA/JPL, and has utilized the NUSTARDAS software package, jointly developed by the ASDC (Italy) and Caltech (USA). This research has also made use of data obtained with *XMM-Newton*, an ESA science mission with instruments and contributions directly funded by ESA Member States. A.L. and S.T. acknowledge support from Russian Science Foundation (grant 14-12-01287).

Facilities: NuSTAR, *XMM-Newton*.

REFERENCES

An, H., Madsen, K. K., Westergaard, N. J., et al. 2014, Proc. SPIE, 9144, 91441Q
Arnaud, K. A. 1996, adass V, 101, 17
Bildsten, L., Chakrabarty, D., Chiu, J., et al. 1997, ApJS, 113, 367
Bird, A. J., Barlow, E. J., Bassani, L., et al. 2006, ApJ, 636, 765
Boldin, P. A., Tsygankov, S. S., & Lutovinov, A. A. 2013, AstL, 39, 375
Chernyakova, M., Lutovinov, A., Rodríguez, J., & Revnivtsev, M. 2005, MNRAS, 364, 455
Churazov, E., Gilfanov, M., & Revnivtsev, M. 2001, MNRAS, 321, 759
Coleiro, A., Chaty, S., Zurita Heras, J. A., Rahoui, F., & Tomsick, J. A. 2013, A&A, 560, A108
Dickey, J. M., & Lockman, F. J. 1990, ARA&A, 28, 215
Doroshenko, V., Santangelo, A., Doroshenko, R., et al. 2014, A&A, 561, A96
Ghosh, P., & Lamb, F. K. 1979, ApJ, 234, 296
González-Galán, A., Kuulkers, E., Kretschmar, P., et al. 2012, A&A, 537, A66
Haberl, F., Angelini, L., Motch, C., & White, N. E. 1998, A&A, 330, 189
Harrison, F. A., Craig, W. W., Christensen, F. E., et al. 2013, ApJ, 770, 103
Hoshino, M., & Takeshima, T. 1993, ApJL, 411, L79
Jansen, F., Lumb, D., Altieri, B., et al. 2001, A&A, 365, L1
King, A. L., Miller, J. M., Raymond, J., Reynolds, M. T., & Morningstar, W. 2015, arXiv:1508.01181
Klus, H., Ho, W. C. G., Coe, M. J., Corbet, R. H. D., & Townsend, L. J. 2014, MNRAS, 437, 3863
Leahy, D. A., Darbro, W., Elsner, R. F., et al. 1983, ApJ, 266, 160
Lutovinov, A., Tsygankov, S., & Chernyakova, M. 2012, MNRAS, 423, 1978
Lutovinov, A. A., & Tsygankov, S. S. 2009, AstL, 35, 433
Lyubarskii, Y. E. 1997, MNRAS, 292, 679
Masetti, N., Pretorius, M. L., Palazzi, E., et al. 2006, A&A, 449, 1139
Mihara, T., Makishima, K., Ohashi, T., Sakao, T., & Tashiro, M. 1990, Natur, 346, 250
Postnov, K. A., Mironov, A. I., Lutovinov, A. A., et al. 2015, MNRAS, 446, 1013
Reig, P. 2011, Ap&SS, 332, 1
Reig, P., & Roche, P. 1999, MNRAS, 306, 100
Revnivtsev, M., Churazov, E., Postnov, K., & Tsygankov, S. 2009, A&A, 507, 1211
Revnivtsev, M. G., Sazonov, S. Y., Molkov, S. V., et al. 2006, AstL, 32, 145
Tsygankov, S. S., Krivonos, R. A., & Lutovinov, A. A. 2012, MNRAS, 421, 2407
Tsygankov, S. S., & Lutovinov, A. A. 2005, AstL, 31, 88
White, N., Swank, J., & Holt, S. 1983, ApJ, 270, 771